LETTER

doi:10.1038/nature13897

The participation of cortical amygdala in innate, odour–driven behaviour

Cory M. Root[1], Christine A. Denny[2,3,4], René Hen[3,4,5] & Richard Axel[1]

Innate behaviours are observed in naive animals without prior learning or experience, suggesting that the neural circuits that mediate these behaviours are genetically determined and stereotyped. The neural circuits that convey olfactory information from the sense organ to the cortical and subcortical olfactory centres have been anatomically defined[1–3], but the specific pathways responsible for innate responses to volatile odours have not been identified. Here we devise genetic strategies that demonstrate that a stereotyped neural circuit that transmits information from the olfactory bulb to cortical amygdala is necessary for innate aversive and appetitive behaviours. Moreover, we use the promoter of the activity-dependent gene *arc* to express the photosensitive ion channel, channelrhodopsin, in neurons of the cortical amygdala activated by odours that elicit innate behaviours. Optical activation of these neurons leads to appropriate behaviours that recapitulate the responses to innate odours. These data indicate that the cortical amygdala plays a critical role in generating innate odour-driven behaviours but do not preclude its participation in learned olfactory behaviours.

Odours can elicit an array of innate behaviours including feeding, mating, freezing or escape, responses essential for the survival and reproduction of the organism. Innate responses to odours can be mediated by either the vomeronasal or main olfactory system[4]. The vomeronasal organ recognizes non-volatile odorants, including the major urinary proteins[5] and steroids[6], that elicit innate responses via a circuit emanating from the accessory olfactory bulb. The main olfactory system recognizes volatile cues including 2,3,5-trimethyl-3-thiazoline (TMT) in fox secretions[7] and trace amines in bobcat[8] and mouse[9] urine that elicit innate attraction and avoidance responses.

Olfactory perception is initiated by the recognition of odorants by a large repertoire of receptors in the sensory epithelium[10–12]. Neurons expressing a given receptor are randomly distributed within zones of the epithelium but project with precision to two spatially invariant glomeruli in the olfactory bulb[13–15]. Thus a transformation in the representation of olfactory information is apparent in the bulb where the dispersed population of active neurons in the sense organ is consolidated into a discrete spatial map of glomerular activity[16]. This invariant glomerular map in the bulb is transformed in the representations in higher olfactory centres. Anatomical tracing experiments reveal that the projections from the olfactory bulb to the cortical amygdala retain a topographic map with individual glomeruli projecting to broad but spatially invariant loci[1]. In contrast, spatial order in the bulb is discarded in the piriform cortex; axons from individual glomeruli project diffusely to the piriform cortex without apparent spatial preference[1–3]. The identification of a distributive pattern of projections to the piriform cortex and stereotyped projections to the cortical amygdala provides an anatomical substrate for the generation of learned and innate behaviours. We have devised behavioural assays and genetic strategies to identify the olfactory centres responsible for innate odour-driven behaviours.

Innate behaviours are often complex and comprise multiple components, but can be simplified by the design of assays that categorize behaviours by only a single axis, positive or negative valence. We therefore developed an open field behavioural assay to determine whether a given odour elicits attraction or avoidance as a measure of innate odour valence. A symmetrical chamber was constructed with four quadrants allowing independent airflow into each of the quadrants with a vacuum in the centre. In the absence of odour, mice explored the chamber without bias for any quadrant (Extended Data Fig. 1f). However, the addition TMT to one quadrant resulted in significant avoidance (Fig. 1a and Extended Data Fig. 1).

We describe the valence of behavioural response to an odour by defining a performance index (see legend to Fig. 1), such that a negative value indicates avoidance and a positive value indicates attraction. In this behavioural assay, TMT revealed a performance index of -83 ± 5.0 ($n = 5$). TMT not only elicited avoidance, but also sitting in distant quadrants, resulting in a marked decrease in locomotor activity, which may be a proxy for freezing (Extended Data Fig. 1e, h). This behavioural assay was used to examine the response of mice to several odorants. We observed that a small group of odorants elicited reliable approach or avoidance behaviour, but most odours elicited no significant behavioural response (Fig. 1b). For example, peanut oil and 2-phenylethanol, a component of rose oil, elicited attraction (performance index 50 ± 4.1 and 49 ± 4.8 ($n = 5$) respectively), whereas the odorants TMT, isopentalamine and 4-methylthiazole elicited aversion (performance index -83 ± 5.0, -81 ± 4 and -59 ± 8.1 ($n = 4$) respectively). Most odours were neutral in this assay and revealed values of performance index near zero, ranging from -7 to 9. Therefore, this robust assay is able to classify the innate valence of odours in terms of approach and avoidance responses.

We have used this behavioural assay in concert with optogenetic silencing to identify a higher olfactory centre necessary for innate olfactory-driven behaviours. The mitral and tufted cells of the olfactory bulb project axons to at least five brain regions[1]: piriform cortex, cortical amygdala, entorhinal cortex, accessory olfactory nucleus and olfactory tubercle. We expressed the light-activated chloride pump, halorhodopsin[17], in neurons of the olfactory bulb to permit optical silencing of the individual projections to these olfactory centres and examined the consequences on innate odour-driven behaviours.

Bilateral injection of an adeno-associated virus (AAV) encoding halorhodopsin fused to enhanced yellow fluorescent protein (AAV-syn-eNpHR3.0–eYFP) resulted in expression in the vast majority of mitral cells in the olfactory bulb (80% ± 7 (s.d.); Fig. 2a, b). Intrinsic neurons within the bulb also expressed halorhodopsin–eYFP, but mitral and tufted cells provide the only feed-forward excitatory output to cortical centres. In initial experiments, we asked whether silencing of neurons within the olfactory bulb suppressed the innate behaviour elicited by TMT. After bilateral infection, both olfactory bulbs were illuminated by introducing optical fibres coupled to a 561 nm laser above the dorsal surface of

[1]Department of Neuroscience and the Howard Hughes Medical Institute, College of Physicians and Surgeons, Columbia University, New York, New York 10032, USA. [2]Department of Biological Sciences, New York State Psychiatric Institute, New York, New York 10032, USA. [3]Department of Neuroscience and Psychiatry, New York State Psychiatric Institute, New York, New York 10032, USA. [4]Division of Integrative Neuroscience, New York State Psychiatric Institute, New York, New York 10032, USA. [5]Department of Pharmacology, Columbia University, New York State Psychiatric Institute, New York, New York 10032, USA.

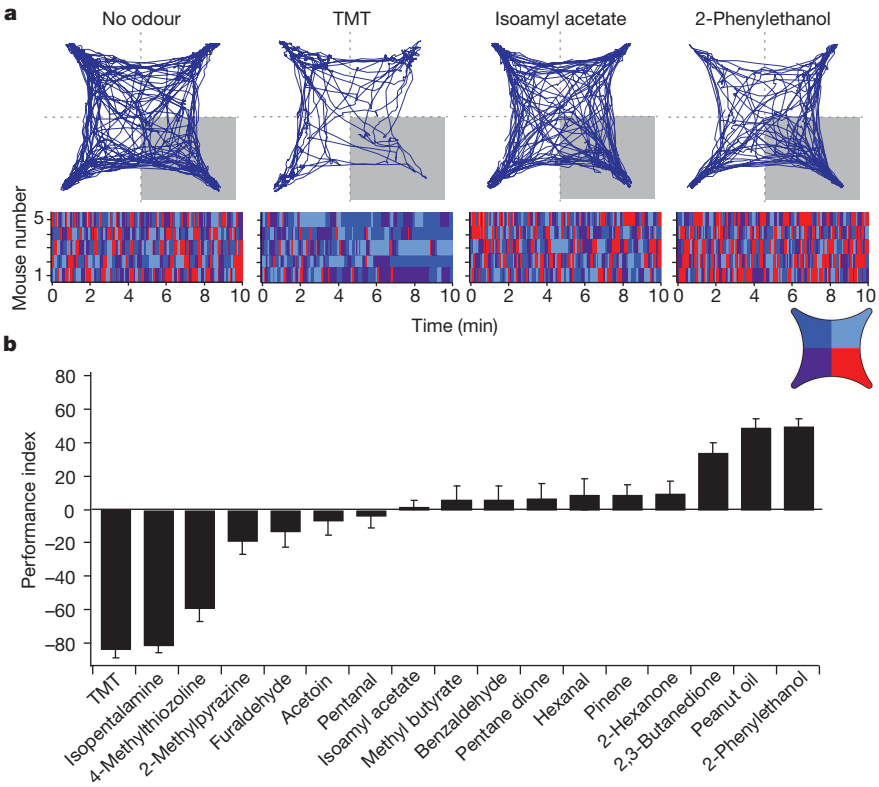

Figure 1 | Behavioural assay for innate responses to odour. An open field, four-quadrant behavioural chamber was used to measure the response to odour delivered in only one quadrant. **a**, The trajectory of a representative mouse is plotted for a 10 minute period in the absence of odour or after the addition of odour to the lower right quadrant. The raster plots below the trajectory graphs represent quadrant occupancy over time (*x* axis) for each of five different animals. The four colours represent occupancy in each of the four quadrants. Odour was delivered to the lower right quadrant (red). **b**, The average response to an array of odorants is quantified by a performance index that represents the percentage difference from chance occupancy in the lower right quadrant (performance index = $(P - 25)/0.25$, where P is the percentage time in the lower right quadrant). One-way analysis of variance (ANOVA) test, $P < 0.001$; $n = 4$–8 for each odour.

the bulb. Previous experiments suggest that the glomeruli responsible for innate behaviour are restricted to the dorsal bulb[7]. Mice were then introduced into the behavioural chamber in which TMT was present within one quadrant and innate aversion was examined in the absence or presence of 561 nm illumination to silence bulbar activity. We observed that light-activated silencing of the olfactory bulb significantly suppressed the aversion to TMT with a reduction in the performance index from -82 ± 3.8 to -18 ± 2.9 ($n = 3$). These experiments demonstrate that these viral injections into the bulb result in halorhodopsin expression in neurons essential for innate aversive behaviour.

We then used optical silencing of the individual targets[18] of the olfactory bulb to identify the olfactory centres necessary to elicit innate behaviour. Photostimulation of the cortical amygdala (Extended Data Fig. 2), for example, in mice expressing halorhodopsin in bulbar neurons should selectively silence bulbar input to this brain structure without affecting input to other olfactory centres. Mice were coupled to a 561 nm laser and placed in the four-field behavioural assay with TMT in a single quadrant. Each of eleven mice exhibited a striking reduction in the avoidance of the TMT quadrant upon bilateral illumination of the cortical amygdala (performance index -65 ± 3.4 without photostimulation, and -7.9 ± 8.4 upon optical silencing) (Fig. 2d). Further, silencing bulbar input significantly reduced the freezing behaviour, as evidenced by decreased bouts of inactivity (Extended Data Fig. 3). The inhibition of innate avoidance observed upon optical silencing of the cortical amygdala was reversible; robust avoidance re-emerged upon cessation of light-induced silencing (performance index -74 ± 5.7). In control animals not injected with virus, aversive behaviour was not impaired by photostimulation (Fig. 2f). We determined the efficacy of silencing upon illumination of bulbar axons by analysing *c-fos* activity. We observe a 70% reduction in the frequency of cells activated by odour in cortical amygdala but not olfactory tubercle or piriform cortex (Extended Data Fig. 4). These results demonstrate that axonal silencing is sufficient and suggests that antidromic hyperpolarization is not responsible for the suppression of behaviour.

We next determined whether input from the olfactory bulb to cortical amygdala is also required for innate attraction. We observed that light-induced silencing of olfactory input to cortical amygdala eliminated attraction to 2-phenylethanol (performance index without photostimulation, 48 ± 3.2; performance index with photostimulation, -8.3 ± 2.1) (Fig. 2e, g and Extended Data Fig. 3b, d), but attraction resumed upon cessation of optical silencing. Thus, input from the olfactory bulb to the cortical amygdala is required to elicit innate responses to both appetitive and aversive odours.

We also asked whether suppression of olfactory input to either piriform cortex or olfactory tubercle, two additional targets of the bulb, would suppress innate, odour-driven behaviours. Bilateral illumination of axons from the olfactory bulb to either the tubercle or the piriform failed to suppress the innate aversion to TMT (performance index -61 ± 3.4 and -67 ± 4.0 respectively, $n = 7$ and 8) (Fig. 2f). Conclusions from these experiments, however, must be tempered by the fact that olfactory inputs to both the tubercle and piriform are extensive and the area of illumination might have been inadequate to suppress axonal input significantly. Nonetheless, this result provides an additional control for antidromic suppression of mitral and tufted cell activity that would result in suppression of innate behaviour independent of the site of optical silencing.

These observations predict that silencing of neurons intrinsic to the cortical amygdala should also inhibit innate behaviour. Halorhodopsin was therefore expressed in the neurons of the cortical amygdala after bilateral injections of AAV-eNpHR3.0–eYFP and bilaterally implanted optical fibres (Extended Data Fig. 5). In each of five mice, we observed a significant decrease in aversion of the TMT quadrant in the four-field behavioural assay (performance index before stimulation, -70 ± 4.8; after photostimulation, -15 ± 7.1) (Fig. 2f). Thus, light-induced silencing of the olfactory bulb, the bulbar projections to cortical amygdala or the neurons of the cortical amygdala dramatically impairs innate aversion to TMT.

Our data suggest that distinct cell populations that reside within the cortical amygdala are capable of eliciting innate responses to either appetitive or aversive odours. We next identified and manipulated the activity of these neurons by exploiting the promoter of the activity-dependent gene *arc*[19], to drive the expression of the light-activated cation channel channelrhodopsin[20]. AAV encoding a Cre-dependent channelrhodopsin fused to the fluorescent protein eYFP (AAV-ef1α-DIO-ChR2–eYFP)

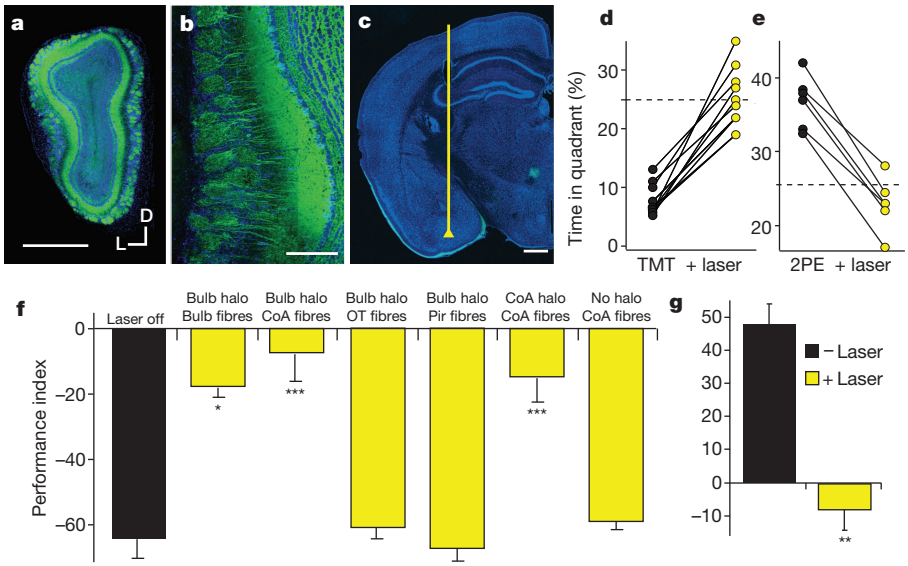

Figure 2 | The projections from the olfactory bulb to cortical amygdala are required for innate aversion and attraction to odours. **a**, Coronal section of a mouse olfactory bulb injected with AAV5-eNpHR3.0–eYFP. D, dorsal; L, lateral. **b**, Magnified view of an olfactory bulb showing eNpHR3.0–eYFP expression in mitral cells. **c**, Coronal section depicting the placement of an optical fibre in cortical amygdala, above the axonal output from the olfactory bulb. Scale bars, 500 μm (**a**, **c**) and 100 μm (**b**). **d**, **e**, Mice were optically coupled to a yellow laser and tested in the behavioural assay for the response to TMT (**d**) or 2-phenylethanol (2PE) (**e**) with and without laser stimulation. The charts show the percentage time each animal spent in the odour quadrant in the absence or presence of photoactivation. **f**, The mean performance index for mice exposed to TMT. The black bar indicates the average response of all mice to TMT in the absence of photoactivation; the yellow bars indicate responses to TMT with photoactivation for different experimental animals. Bulb halo and CoA halo describe mice with halorhodopsin expression in the olfactory bulb and cortical amygdala, respectively. Optical fibres were placed above the bulb ($n = 3$), cortical amygdala (CoA, $n = 11$), olfactory tubercle (OT, $n = 7$) or in piriform cortex (Pir, $n = 8$) as denoted below the site of injection. The last two bars on the right side have either halorhodopsin in the neurons of cortical amygdala ($n = 5$), or receive no viral injection ($n = 4$), and fibres implanted into cortical amygdala. **g**, The mean performance index for mice exposed to 2-phenylethanol in the absence and presence of photoactivation ($n = 6$). **f**, **g**, $^{*}P < 0.05$, $^{**}P < 0.01$, $^{***}P < 0.001$, paired *t*-test comparing performance index with and without laser for each group; error bars, s.e.m.

was injected into the cortical amygdala of mice harbouring a transgene in which the *arc* promoter drives the expression of the tamoxifen-sensitive Cre-recombinase ($CreER^{T2}$) (Fig. 3a). In this $ArcCreER^{T2}$ mouse[21], neuronal activation should result in the expression of $CreER^{T2}$. In the presence of tamoxifen, activated Cre will effect the recombination between the loxP sites of AAV-ef1α-DIO-ChR2, resulting in the irreversible expression of ChR2–eYFP. The fusion of Cre with the tamoxifen-sensitive oestrogen receptor allows temporal control of the recombination activity. Thus administration of tamoxifen followed by exposure to odour should result in the expression of ChR2–eYFP in the neurons activated by the odour (Fig. 3b, c), permitting us to mark and manipulate the activity of these neural populations.

In initial experiments, we determined whether ChR2–eYFP is faithfully expressed in neurons that respond to specific odours in the cortical amygdala. ChR2–eYFP should be expressed by neurons responsive to TMT and subsequent re-exposure of the mice to TMT should result in the acute expression of endogenous arc in ChR–eYFP positive neurons. This temporal separation permitted us to identify populations of neurons activated by sequential stimuli in the same animal and to determine whether the expression of ChR2–eYFP is a faithful reporter of endogenous *arc* activity. We observed that 80% ± 5.9 (s.d.) of the ChR2–eYFP+ neurons also expressed endogenous arc ($n = 4$). About 50% of the neurons expressing endogenous arc also expressed ChR2–eYFP (Extended Data Fig. 6a, c). These results indicate that the expression of ChR2–eYFP is a faithful reporter of endogenous *arc* activity, identifying a population of neurons responsive to TMT.

We next asked whether odours that elicit innate behaviours of different valence activate different populations of neurons in the cortical amygdala. AAV encoding Cre-dependent ChR2 was injected into the cortical amygdala of $ArcCreER^{T2}$ mice. After tamoxifen treatment, the mice were sequentially exposed to the attractive odour 2-phenylethanol and the aversive odour TMT. In this experimental design, the neurons responsive to 2-phenylethanol will express ChR2–eYFP, whereas the neurons responsive to TMT will express the endogenous arc. Only 4% ± 2.1 (s.d.) of the ChR2–eYFP+ neurons activated by 2-phenylethanol also expressed endogenous arc, activated by TMT ($n = 4$) (Extended Data Fig. 6b, c). These data suggest that odours that elicit appetitive and aversive innate behaviours activate different populations of neurons in the cortical amygdala that can be faithfully identified and manipulated after AAV infection of an $ArcCreER^{T2}$ mouse.

The $ArcCreER^{T2}$ mice were used to determine whether the cortical amygdala is sufficient to elicit a response that recapitulates the behaviour observed with odour. We therefore injected AAV encoding Cre-dependent ChR2–eYFP into the cortical amygdala of $ArcCreER^{T2}$ mice and optical fibres were implanted unilaterally above the injection site. Mice were treated with tamoxifen and then exposed to odour. We observed ChR2 expression in cortical amygdala and neighbouring areas of piriform cortex and medial amygdala. However, c-fos staining demonstrated that optical activation is restricted to cortical amygdala as a consequence of fibre placement (Extended Data Fig. 7b). Behavioural assays were performed in the four-field arena, but odour was not placed in one quadrant: rather, the entrance to a single quadrant triggered pulsed laser stimulation via a custom closed-loop computer program.

Photoactivation of the cortical amygdala of mice expressing ChR2 after TMT exposure resulted in avoidance of the optically stimulated quadrant (performance index −49 ± 4.6, $n = 6$) (Fig. 3d, g) and increased freezing as evidenced by increased immobility (Extended Data Fig. 8). In contrast, mice expressing ChR2 in neurons responsive to the innately attractive odour 2-phenylethanol exhibited significant attraction to the quadrant in which the mice received optical stimulation (performance index 42 ± 6.4, $n = 4$) (Fig. 3e, g). Mice expressing channelrhodopsin in neurons responsive to the neutral odour isoamyl acetate did not exhibit any discernible behavioural response upon optical stimulation (performance index 5.6 ± 8.6, $n = 6$) and explored each quadrant equally

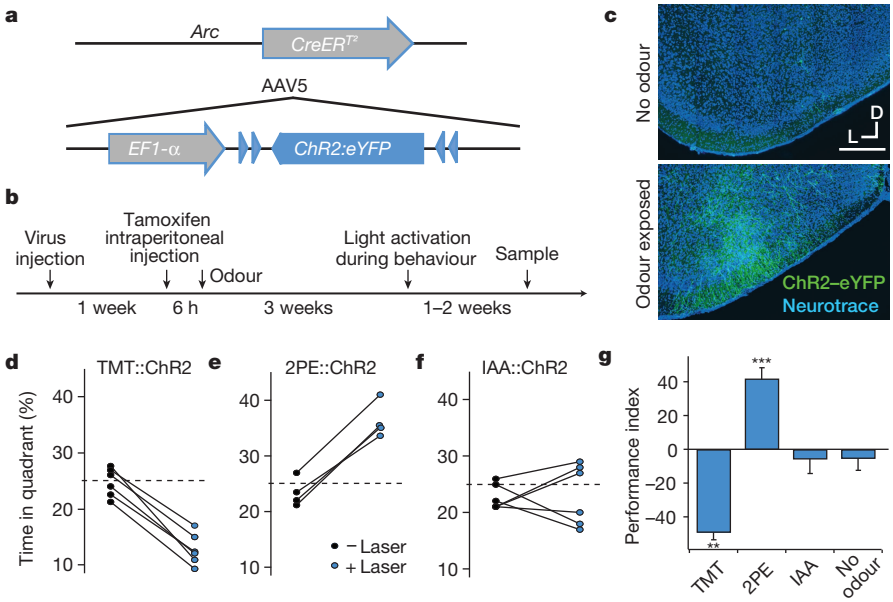

Figure 3 | Activation of odour-responsive neurons within cortical amygdala is sufficient to recapitulate behavioural responses. **a**, The genetic strategy used to express ChR2 in odour-responsive neurons. The tamoxifen-sensitive Cre recombinase CreER^{T2} was expressed under the control of the promoter of the activity-dependent gene, *arc*, in a transgenic mouse. The gene encoding Cre-dependent ChR2–eYFP was introduced into the cortical amygdala by infection with AAV5. **b**, The timeline for experimental manipulations. The animal was sampled upon termination of behavioural testing. **c**, Representative images showing the expression of ChR2–eYFP in mice that received tamoxifen injection followed by exposure to either the odorant isoamyl acetate (bottom) or no odour as a control (top). Scale bar, 300 μm. **d**–**f**, Mice with odour-driven channelrhodopsin expression were tested in the open field assay where they received pulsed photoactivation upon entrance into one quadrant. The percentage time each animal spent in the lower right quadrant in the absence and presence of pulsed photoactivation in mice with neurons activated by TMT (**d**), 2-phenylethanol (**e**) and isoamyl acetate (IAA) (**f**). **g**, The average performance index for mice receiving photostimulation of neurons activated by TMT, 2-phenylethanol, isoamyl acetate or no odour, respectively, from left to right ($n = 3$–6). $^{**}P < 0.01$, $^{***}P < 0.001$, *t*-test comparing performance index with and without laser; error bars, s.e.m.

(Fig. 3f, g). In control mice, treatment with tamoxifen without odour exposure resulted in ChR2 expression in a very small subpopulation of neurons. These mice did not exhibit any behavioural bias upon photostimulation within a single quadrant (performance index -5.2 ± 7.1, $n = 3$) (Fig. 3g). These experiments demonstrate that odours that elicit innate behaviours of different valence activate different populations of neurons within the cortical amygdala. Moreover, photoactivation of these two distinct populations of neurons is sufficient to elicit an appropriate behavioural response. Thus, these neural representations reflect an essential component in a determined neural circuit wired to elicit an innate behavioural response to odours.

The presence of spatially stereotyped projections from individual glomeruli to the cortical amygdala[1] suggest that the neural representations activated by aversive and attractive odours may be anatomically segregated. We therefore examined the spatial distribution of neurons activated by odour after AAV infection of the ArcCreER^{T2} mouse (Fig. 4a, b and Extended Data Fig. 9). We observed that the ChR2–eYFP^{+} neurons, activated by the appetitive odours, 2-phenylethenol and peanut oil, were most abundant in the caudal third of the posterolateral cortical amygdala. Sparse labelling was observed in more anterior regions. In contrast, the aversive odours TMT, isopentylamine and 4-methylthiozoline activated neurons distributed throughout the cortical amygdala. Significant labelling was observed in more anterior regions that were not activated by odours that elicited appetitive behaviours. Neutral odours such as isoamyl acetate also failed to activate neurons in the anterior region and revealed labelling in a pattern not dissimilar from that observed with appetitive odours.

A given odour, even those that elicit innate behaviours, may activate as many as 100 glomeruli, and the inputs from these glomeruli may activate neurons distributed diffusely across the cortical amygdala. Neurons in the most anterior portion of the cortical amygdala, however, may only be activated by odours that elicit innate aversive behaviours. Our data suggest a model in which aversive odours activate a small subset of glomeruli that project to anterior cortical amygdala and a larger set of glomeruli that project more broadly throughout the cortical amygdala. Regions responsible for appetitive behaviours may reside in more posterior domains; however, a locus that is uniquely responsive to appetitive odours is not easily distinguishable in our analyses. Neurons in the cortical amygdala are also activated by neutral odours that do not elicit an apparent behavioural response. We do not know the functional significance of the neural representation of neutral odours. These neurons may also reside in segregated domains that encode innate features of an odour, including subtle behaviours or odour quality, that are not discernible in our assays. Alternatively, the neurons in cortical amygdala responsive to neutral odour may participate in the adaptive response to odours, a function thought to engage the piriform cortex[22].

The response to most odours is not innate but adaptive. Most odours have predictive value only over the lifetime of the organism and acquire meaning through learning, a function suited to the unstructured representation in piriform cortex[23–25]. Exogenous activation of an arbitrarily chosen ensemble of piriform neurons can result in appetitive, aversive and social behaviours only after associative learning[22]. Therefore, odour representations in piriform cortex are afforded behavioural significance upon experience. Our data indicate that the cortical amygdala plays a critical role in the generation of innate odour-driven behaviours but do not preclude the participation of cortical amygdala in learned olfactory behaviours. Cortical amygdala may cooperate with piriform cortex to impose meaning on a random ensemble of active neurons in piriform. One major target of piriform output is the cortical amygdala[26]. Piriform connections in the cortical amygdala may therefore exploit the distinct subpopulations of neurons in cortical amygdala capable of eliciting innate behaviours to generate learned responses to odour. In one model, direct connections from the olfactory bulb to cortical amygdala may elicit innate odour-driven behaviours, whereas indirect connections from the bulb through piriform to cortical amygdala may elicit learned responses to odour. This indirect, trisynaptic pathway may facilitate

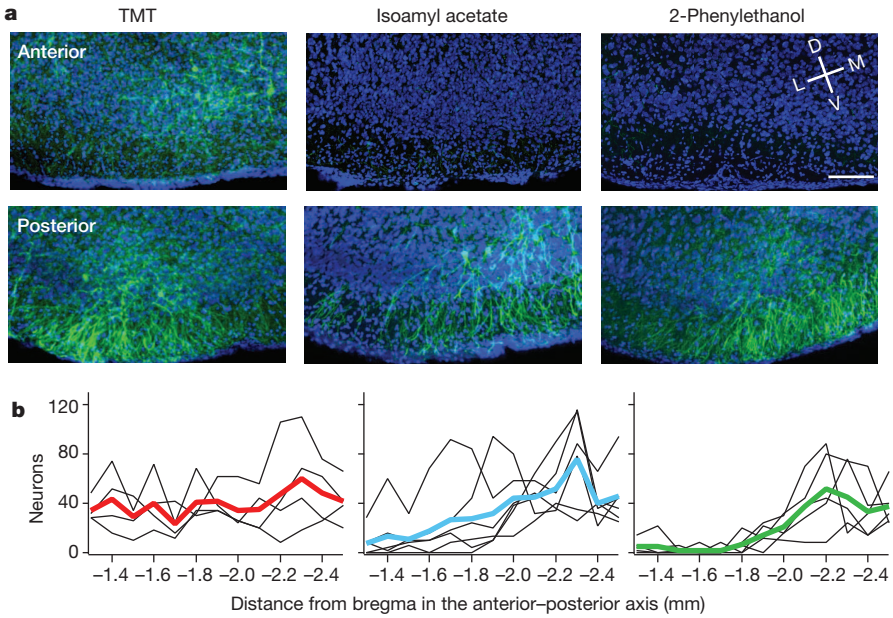

Figure 4 | The spatial distribution of neurons responsive to different odours within the cortical amygdala. ArcCreER^{T2} mice were administered tamoxifen and exposed to one of three different odours and then consecutive, serial, coronal sections were collected throughout the cortical amygdala region. **a**, Images reveal odour-driven ChR2–eYFP expression in representative images of anterior (top) and posterior (bottom) cortical amygdala for each odour. Images of the ventral brain region are magnified and cropped to show only the posterolateral cortical amygdala, and sections are displayed at −1.4 and −2.2 mm relative to bregma. Scale bar, 100 μm. D, dorsal; L, lateral; M, medial; V, ventral. **b**, The number of neurons counted per 100 μm throughout the posterolateral cortical amygdala is displayed for each odour. The number for each animal is indicated with a thin black line; the heavier coloured line shows the mean for the odour group ($n = 4$–6).

learning-dependent synaptic changes necessary to impart valence on a random ensemble of neurons. The convergence of direct monosynaptic input and indirect polysynaptic input, capable of more complex computations from the same brain structure, is a common motif both in vertebrate[27] and invertebrate[28] brains.

Online Content Methods, along with any additional Extended Data display items and Source Data, are available in the online version of the paper; references unique to these sections appear only in the online paper.

Received 4 April; accepted 26 September 2014.
Published online 5 November 2014.

1. Sosulski, D. L., Bloom, M. L., Cutforth, T., Axel, R. & Datta, S. R. Distinct representations of olfactory information in different cortical centres. *Nature* **472,** 213–216 (2011).
2. Miyamichi, K. *et al.* Cortical representations of olfactory input by trans-synaptic tracing. *Nature* **472,** 191–196 (2011).
3. Ghosh, S. *et al.* Sensory maps in the olfactory cortex defined by long-range viral tracing of single neurons. *Nature* **472,** 217–220 (2011).
4. Stowers, L. & Logan, D. W. Olfactory mechanisms of stereotyped behavior: on the scent of specialized circuits. *Curr. Opin. Neurobiol.* **20,** 274–280 (2010).
5. Chamero, P. *et al.* Identification of protein pheromones that promote aggressive behaviour. *Nature* **450,** 899–902 (2007).
6. Nodari, F. *et al.* Sulfated steroids as natural ligands of mouse pheromone-sensing neurons. *J. Neurosci.* **28,** 6407–6418 (2008).
7. Kobayakawa, K. *et al.* Innate versus learned odour processing in the mouse olfactory bulb. *Nature* **450,** 503–508 (2007).
8. Dewan, A., Pacifico, R., Zhan, R., Rinberg, D. & Bozza, T. Non-redundant coding of aversive odours in the main olfactory pathway. *Nature* **497,** 486–489 (2013).
9. Li, Q. *et al.* Synchronous evolution of an odor biosynthesis pathway and behavioral response. *Curr. Biol.* **23,** 11–20 (2013).
10. Buck, L. & Axel, R. A novel multigene family may encode odorant receptors: a molecular basis for odor recognition. *Cell* **65,** 175–187 (1991).
11. Godfrey, P. A., Malnic, B. & Buck, L. B. The mouse olfactory receptor gene family. *Proc. Natl Acad. Sci. USA* **101,** 2156–2161 (2004).
12. Zhang, X. & Firestein, S. The olfactory receptor gene superfamily of the mouse. *Nature Neurosci.* **5,** 124–133 (2002).
13. Ressler, K. J., Sullivan, S. L. & Buck, L. B. Information coding in the olfactory system: evidence for a stereotyped and highly organized epitope map in the olfactory bulb. *Cell* **79,** 1245–1255 (1994).
14. Mombaerts, P. *et al.* Visualizing an olfactory sensory map. *Cell* **87,** 675–686 (1996).
15. Vassar, R. *et al.* Topographic organization of sensory projections to the olfactory bulb. *Cell* **79,** 981–991 (1994).
16. Rubin, B. D. & Katz, L. C. Optical imaging of odorant representations in the mammalian olfactory bulb. *Neuron* **23,** 499–511 (1999).
17. Gradinaru, V., Thompson, K. R. & Deisseroth, K. eNpHR: a Natronomonas halorhodopsin enhanced for optogenetic applications. *Brain Cell Biol.* **36,** 129–139 (2008).
18. Tye, K. M. *et al.* Amygdala circuitry mediating reversible and bidirectional control of anxiety. *Nature* **471,** 358–362 (2011).
19. Link, W. *et al.* Somatodendritic expression of an immediate early gene is regulated by synaptic activity. *Proc. Natl Acad. Sci. USA* **92,** 5734–5738 (1995).
20. Boyden, E. S., Zhang, F., Bamberg, E., Nagel, G. & Deisseroth, K. Millisecond-timescale, genetically targeted optical control of neural activity. *Nature Neurosci.* **8,** 1263–1268 (2005).
21. Denny, C. A. *et al.* Hippocampal memory traces are differentially modulated by experience, time, and adult neurogenesis. *Neuron* **83,** 189–201 (2014).
22. Choi, G. B. *et al.* Driving opposing behaviors with ensembles of piriform neurons. *Cell* **146,** 1003–1014 (2011).
23. Stettler, D. D. & Axel, R. Representations of odor in the piriform cortex. *Neuron* **63,** 854–864 (2009).
24. Poo, C. & Isaacson, J. S. Odor representations in olfactory cortex: "sparse" coding, global inhibition, and oscillations. *Neuron* **62,** 850–861 (2009).
25. Illig, K. R. & Haberly, L. B. Odor-evoked activity is spatially distributed in piriform cortex. *J. Comp. Neurol.* **457,** 361–373 (2003).
26. Schwabe, K., Ebert, U. & Loscher, W. The central piriform cortex: anatomical connections and anticonvulsant effect of GABA elevation in the kindling model. *Neuroscience* **126,** 727–741 (2004).
27. Tonegawa, S. & McHugh, T. J. The ins and outs of hippocampal circuits. *Neuron* **57,** 175–177 (2008).
28. Tanaka, N. K., Tanimoto, H. & Ito, K. Neuronal assemblies of the *Drosophila* mushroom body. *J. Comp. Neurol.* **508,** 711–755 (2008).

Acknowledgements We thank L. Abbott, T. Jessell and D. Costantini for comments and reading the manuscript; B. Bader for assistance with experiments; M. Mendelsohn and N. Zabello for help with mice; P. Kisloff for assistance in preparation of the manuscript; and A. Nemes and M. Gutierrez for laboratory support. This work was supported by the Howard Hughes Medical Institute and the Mathers Foundation.

Author Contributions C.M.R. and R.A. conceived the project, participated in its development, wrote the manuscript and analysed data. C.M.R. performed all experiments. C.A.D. and R.H. conceived and generated the ArcCreER^{T2} transgenic mouse.

Author Information Reprints and permissions information is available at www.nature.com/reprints. The authors declare no competing financial interests. Readers are welcome to comment on the online version of the paper. Correspondence and requests for materials should be addressed to R.A. (ra27@columbia.edu).

METHODS

Behavioural assay. The four-field behaviour chamber was inspired by similar assays used in experiments with *Drosophila* (see refs 29–31). The custom behavioural chamber was machined from plastic materials with the help of the Columbia University machine shop on the Nevis campus. The chamber was an enclosed four-quadrant arena with airflow into the centre and a vacuum in the middle. Airflow at 150 ml min^{-1} aws pumped into each quadrant via gas-mass flow controllers (Cole-Parmer). Airflow exited the chamber via a 1-inch outlet in the centre of the floor covered by steel mesh. The outlet was connected a vacuum line with a gas-mass controller set to 700 ml min^{-1}. The chamber had a 76 cm diameter, a corner arc of 1.9 cm radius and a chamber height of 7.6 cm. The floor and the walls were made out of polypropylene and the hinged ceiling was clear, ½-inch thick acrylic. Odour was applied by solenoid valves redirecting airflow through 100 ml glass bottles containing 1 µl of pure odorant on a small piece of Kimwipe. The chamber was housed in a dark environment and illuminated by infrared lights below the floor. A Basler A601FM camera (Edmund Optics) mounted above the chamber recorded the animals' behaviour. Custom software written in Labview (National Instruments) tracked the position of the mouse in real time at a rate of 4 Hz. The behaviour was further analysed offline using custom, unbiased scripts written in Igor Pro (Wavemetrics).

Mice were placed in the chamber for 25 min experiments and tested only once per day. The first 10 min served as a baseline test for bias within the arena. The first 2 minutes of data after the odour was introduced were excluded from the analysis to reduce variance without affecting the overall valence of the behavioural response. The symmetrical behaviour chamber was contained in a lightproof structure and illuminated by infrared lights. Therefore, there were no spatial cues available to the animals with respect to the room, and the odour was always delivered in the same quadrant. To control for any spatial bias, animals were always tested with a 10 min period of no odour. If an animal avoided any one quadrant more than 20% from chance, the experiment was terminated and the animal was tested again on another day. For the experiments in Fig. 1, this occurred in fewer than 10% of the trials and a given animal was never excluded from the data set. For the optogenetic experiments, mice were more inclined to sessions of inactivity resulting in bias for one area during the baseline period. Repeated baseline testing acclimated the animals to being tethered in the chamber, which typically permitted the experiment to proceed after one or two baseline sessions. About half of the animals required more than one baseline period before the experiment could continue. Of the 65 mice tested in the optogenetic experiments, only four were rejected because of unremitting problems with locomotor activity or spatial bias during the baseline period. Moreover, we observed that a given animal could be retested to the same odour at least five times on consecutive days and exhibited no experience-dependent bias during the baseline, and then exhibited reliable responses to the odour (data not shown). Therefore, mice did not exhibit any signs of conditioned place preference or learned responses to odour in this assay. Experiments in Fig. 1a–d were performed with the same set of animals, and those in Fig. 1e were obtained from overlapping groups of animals. Odours were tested in random order. A preliminary set of experiments revealed that, depending on the variance and magnitude of difference, a sample as small as four animals was sufficient to achieve significant findings.

Optogentic behaviour experiments. Animals were only tested once per day, and the laser on/off sessions occurred at least 1 day apart. Half of the mice experienced odour with the laser on upon the first test, and the other half experienced the odour with the laser off first. Mice were implanted with custom-made fibre cannulas assembled as follows. Optical fibres (200 µm, 0.39 numerical aperture, Thorlabs) were epoxied to 2.5 mm stainless steel ferrules (Precision Fibre Products), and polished with a fibre optic polishing kit (Thorlabs) to achieve a minimum of 80% transmission. After surgical implantation, the ferrules protruding from an animal's head could be coupled to either a 100 mW 473 nm or 100 mW 561 nm laser (Shanghai Laser & Optics Century) via custom-made patch cords with either a single, or beam splitting, rotary joint (Doric Lenses) between the mouse and the laser. The fibre was introduced to the behaviour chamber through a 1 cm hole in the left side of the chamber. During the behavioural experiment, it was necessary to pull the slack of the fibre as the mouse traversed the chamber to prevent the mouse from getting tangled in the fibre. Therefore, a motorized pulley system was created to pull the fibre-coupled rotary joint along a vertical tract adjacent to the hole where the fibre entered the chamber. Custom closed-loop software written in Labview monitored the position of the mouse and drove the pulley system to adjust the height of the rotary joint to maintain the appropriate amount of slack. The blue laser was pulsed with 50 ms bins at 10 Hz, and there was a steep gradient from 1 to 10 Hz along the perimeter of the quadrant. The lasers were controlled by transistor–transistor logic (TTL) modulation from custom Labview software.

Light intensity. Fibres were implanted approximately 200–400 µm above layer II of the cortical amygdala, which should have illuminated an area with a radius no more than 600 µm. For halorhodopsin experiments, the 561 nm laser power was adjusted to produce an estimated 10 mW at the implanted fibre tip, which we calculated as providing an irradiance of 9–22 mW mm^{-2} at layer II of the cortical amygdala. Suppression in the olfactory bulb was performed by placing optical fibres bilaterally 0.5–1 mm above the centre of the dorsal surface of the bulb. We estimated the conical spread of light from the fibre tip illuminated an area of about 3.5 mm in diameter with at least 7 mW mm^{-2}. In these experiments, the fibre was introduced through a bilateral cannula positioned in the centre of the olfactory bulbs about 0.5 mm above the surface at coordinates relative to bregma (~5.0 anterior–posterior, 1.0 medial–lateral). The olfactory bulb was roughly 3 mm in length and 1–2 mm wide, so fibres placed above the centre would illuminate most of the dorsal surface. For channelrhopsin experiments, the 473 nm laser was adjusted to an estimated 5–7 mW at the implanted fibre tip, which we calculated as providing an irradiance of 7–18 mW mm^{-2} at layer II of the cortical amygdala. A conservative estimate of the radius of illumination was calculated with trigonometry using the half angle of divergence for a multimode optical fibre: $\theta = \sin^{-1}(\mathrm{NA}/n)$, where NA is the numerical aperture of the fibre (0.39) and n is the index of refraction of grey matter (1.36) (ref. 32). However, it has been suggested that, because of scattering in tissue, the lateral spread is quantitatively similar to the depth of forward light spread from the fibre tip[33]. Thus, at 400 µm below the fibre tip, the radius of illumination would be 400 µm from the fibre edge. Power attenuation was calculated as described[34]:

$$\frac{I_z}{I_{z0}} = \frac{\tilde{n}^2}{(S_z+1)(z+\tilde{n})^2}$$

where $\tilde{n} = r\sqrt{\left(\frac{n}{NA}\right)^2 - 1}$, S_z is the scatter coefficient (11.2) per unit thickness and z is the thickness of the sample.

Experimental subjects. Adult C57BL/6J mice (Jackson laboratory) aged 8–16 weeks old were group housed until surgery and then singly housed on a reverse light cycle. For experiments that did not require surgery, mice were singly housed for at least 5 days before testing. ArcCreER^{T2} mice were group housed until they were 7–9 weeks old when surgeries were performed, after which the mice were singly housed. In the days preceding behavioural experiments, mice were handled regularly to adapt them to the experimenter and the attachment of fibre patch cords. Halorhodopsin experiments began 3–4 weeks after the viral injection to achieve high levels of expression.

Stereotactic surgery. Animals were anaesthetized with ketamine and xylazine (100 mg per kg, 10 mg per kg, respectively, Henry Schein) and placed in a stereotactic frame (Narishige). Small craniotomies were made using standard aseptic technique. Virus was injected with needles pulled from capillary glass (Drummond) at a flow rate of approximately 100 nl min^{-1} by manual pressure injection. Each olfactory bulb received two injections of 1 µl of AAV5-hSyn-eNpHR3.0–eYFP (UNC Viral Core) injected in two locations along the anterior–posterior axis relative to bregma: 5.4 and 6.2 anterior–posterior, 1.1 medial–lateral, −1.4 dorsal–ventral from the bulb surface. Injections into cortical amygdala were also 1 µl in volume at coordinates relative to bregma: −1.7 anterior–posterior, 2.8 medial–lateral, −5.9 dorsal–ventral. Animals exhibited broad expression covering at least 90% of the area of the posterolateral cortical amygdala. For experiments with the ArcCreER^{T2} mice, animals were injected with the Cre-dependent virus: AAV5-ef1α-DIO-hChR2(H134R)–eYFP (UNC Viral Core). Fibres were implanted into the cortical amygdala at about −1.7 anterior–posterior, 2.8 medial–lateral, −5.7 dorsal–ventral for most experiments; however, for experiments with photoactivation of ChR2 in 2-phenylethanol-responsive neurons, the fibres were implanted slightly more posterior (−2.0 anterior–posterior, 2.9 medial–lateral, −5.7 dorsal–ventral). The fibres were fixed in place using a small amount of clear dental cement (CB Metabond, Parkell) covering the surface of the skull, followed by an outer coating of black Ortho Jet dental acrylic (Lang Dental Manufacturing). Buprenorphine (0.05 mg per kg, Henry Schein) was administered. All injection sites and fibre placements were verified histologically and in rare cases mice were excluded if either were mistargeted. All experiments were conducted according to approved protocols at Columbia University.

ArcCreER^{T2} mice. A transgenic mouse was generated from a Bac clone containing the entire *arc* gene (see ref. 21). The mice received viral injections at approximately 8 weeks of age. Five days after injection, mice were dark adapted by placing them in a lightproof chamber with fresh bedding for 36–48 h. On day 7 after injection, mice were administered 2 mg of tamoxifen (Sigma T5648). Tamoxifen was prepared as a 10 mg ml^{-1} stock solution dissolved into a 1:10 mixture of ethanol and corn oil (Sigma C8267) and 0.2 ml was administered by intraperitoneal injection. Six hours after tamoxifen, mice were exposed to odour on a cotton swab placed through the roof of their cage twice for 15 min each during a 1 h period. One microlitre of pure odorant was pipetted onto the cotton swab. Mice were maintained in the dark for an additional 48 h after tamoxifen injection before returning to the reverse light cycle. Photoactivation experiments began 3 weeks after tamoxifen and odour exposure.

Histological processing. Mice were administered ketamine and xylazine (100 mg per kg and 10 mg per kg, respectively) and euthanized by transcardial perfusion with 10 ml of PBS, followed by 10 ml of 4% paraformaldehyde in PBS. Brains were extracted and 100 μm coronal sections were cut on a vibratome. The tissue was labelled with the following antibodies: goat anti-GFP (Abcam ab6673), rabbit anti-arc (Synaptic Systems 156-003), goat anti-c-fos (Santa Cruz sc-52-G), alexa-488 donkey anti-goat (Jackson ImmunoResearch), alexa-568 donkey anti-rabbit (Life Technologies A11057), alexa-647 donkey anti-rabbit (Jackson ImmunoResearch 711-605-152) and alexa-568 donkey anti-goat (Life Technologies A10042). Slices were counterstained with neurotrace 640/660 or 435/455 (Life Technologies N21483 or N21479, respectively). Antibody amplification was not used to visualize eNpHR3.0–eYFP. All images were taken using a Zeiss LSM-710 confocal microscope system.
Cell counting. Confocal images were taken with a ×40 objective and *z*-stacks of approximately 50 μm in depth at a resolution of 256 pixels × 256 pixels. Counting of Chr2–eYFP- and Arc-expressing neurons was performed manually by scrolling through the *z*-stack with tiled regions of interest. We counted neurons expressing c-fos by creating a projection of the *z*-stack, and then counting with an automated program written in Labview. It was not possible to count the ChR2–eYFP-expressing neurons with the automated program because membrane targeting confounds the detection of cell bodies.

29. Louise, E. M., Vet, J. C. V. L., Heymans, M. & Meelis, E. An airflow olfactometer for measuring olfactory responses of hymenopterous parasitoids and other small insects. *Physiol. Entomol.* **8,** 97–106 (1983).
30. Faucher, C., Forstreuter, M., Hilker, M. & de Bruyne, M. Behavioral responses of *Drosophila* to biogenic levels of carbon dioxide depend on life-stage, sex and olfactory context. *J. Exp. Biol.* **209,** 2739–2748 (2006).
31. Semmelhack, J. L. & Wang, J. W. Select *Drosophila* glomeruli mediate innate olfactory attraction and aversion. *Nature* **459,** 218–223 (2009).
32. Vo-Dinh, T. *Biomedical Photonics Handbook* Ch. 2, 37 (CRC, 2003).
33. Yizhar, O., Fenno, L. E., Davidson, T. J., Mogri, M. & Deisseroth, K. Optogenetics in neural systems. *Neuron* **71,** 9–34 (2011).
34. Aravanis, A. M. *et al.* An optical neural interface: in vivo control of rodent motor cortex with integrated fiberoptic and optogenetic technology. *J. Neural Eng.* **4,** S143–S156 (2007).

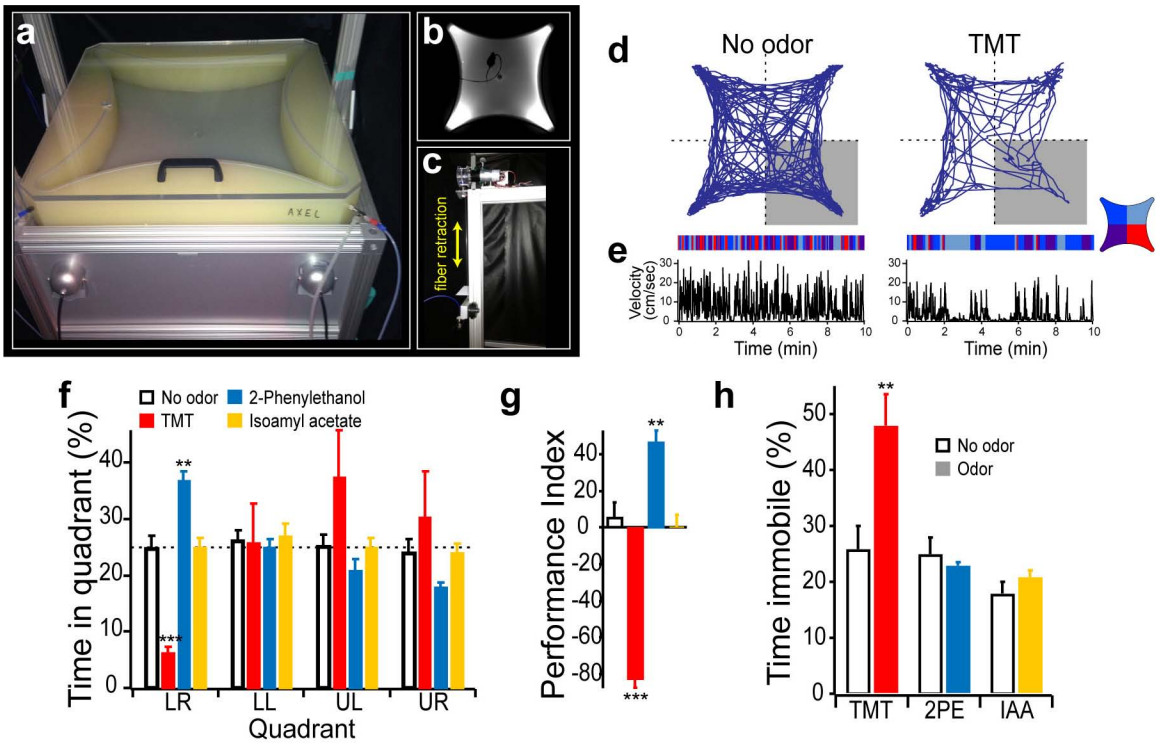

Extended Data Figure 1 | Quantification of the four-quadrant behaviour assay. **a**–**c**, Images of the four-field behaviour chamber. **b**, An image, taken from the camera that tracked the position of the animal, showing a mouse tethered to optic fibres that entered the chamber through a port on the left side. **c**, A motorized fibre retraction system adjusted the length of the fibre as the mouse traversed the arena. The trajectory of a representative mouse is plotted for a 10 minute period in the absence of odour (left), or after the addition of odour to the lower right quadrant (right). The raster plots below the trajectory graphs represent quadrant occupancy over time. **e**, The velocity over time in the absence of odour (left) or in the presence of TMT (right) reveals bouts of inactivity associated with freezing behaviour in the presence of TMT. **f**, The average amount of time spent in each quadrant either in the absence of odour, or the presence of TMT, 2-phenylethanol or isoamyl acetate. **g**, This quantification is reduced when plotted as the performance index ($n = 5$). **h**, Pauses in locomoter activity are quantified as the percentage time immobile in the presence and absence of TMT, 2-phenylethanol or isoamyl acetate. Immobility is defined as velocity less than 1 cm s^{-1} for at least 1 s. **f**–**h**, $^{**}P < 0.01$, $^{***}P < 0.001$, paired *t*-test comparing performance index with and without odour for each odour group; error bars, s.e.m.

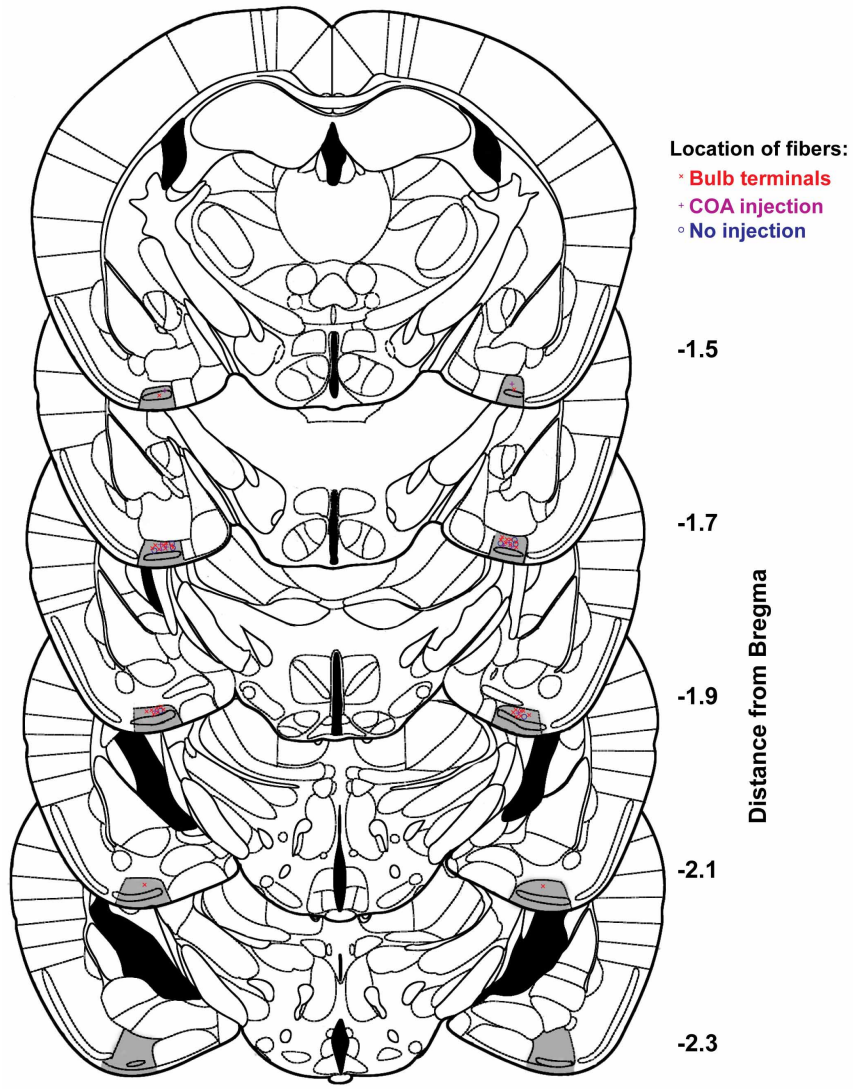

Extended Data Figure 2 | Location of optical fibres implanted in cortical amygdala for photoactivation of halorhodopsin. Schematics show coronal sections throughout most of the region containing cortical amygdala. The posterolateral cortical amygdala is highlighted in grey and the location of bilaterally implanted fibres is indicated.

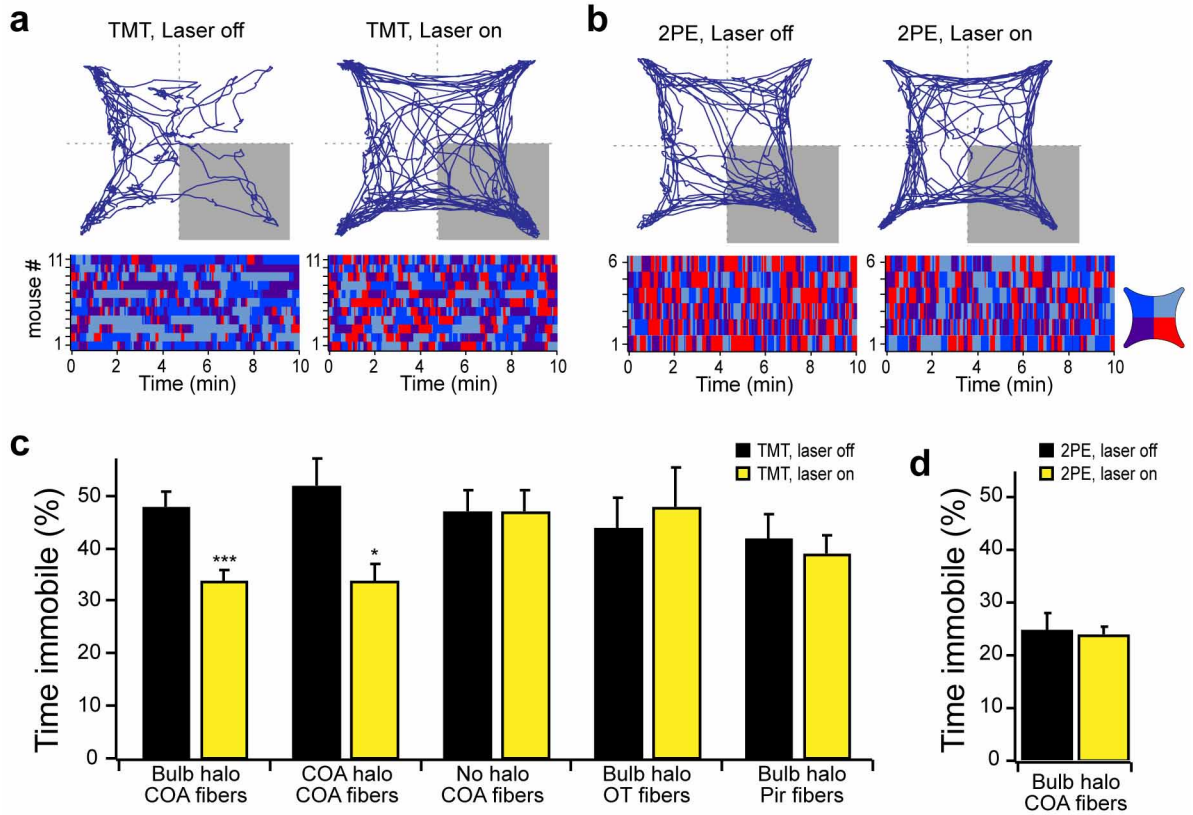

Extended Data Figure 3 | Locomotor activity of mice with optical suppression in cortical amygdala. **a**, **b**, Mice with halorhodopsin in the olfactory bulb and optical fibres in cortical amygdala were optically coupled to a yellow laser and tested in the behavioural assay for the response to TMT (**a**) or 2-phenylethanol (**b**) with and without laser stimulation. The position of a representative mouse during a 10 minute period in the presence of TMT (**a**) or 2-phenylethanol (**b**) either in the absence (left) or presence (right) of photoactivation during the 10 minute behavioural testing is shown. Raster plots show quadrant occupancy over time for each animal (**a**, $n = 11$; **b**, $n = 6$). **c**, **d**, The percentage time immobile in the absence and presence of photoactivation. Immobility is defined as velocity less than 1 cm s^{-1} for at least 1 s. **c**, Response to TMT in mice receiving photostimulation of halorhodopsin in different experimental animals. Bulb halo and COA halo describe mice with halorhodopsin expression in the olfactory bulb and cortical amygdala, respectively. Optical fibres were placed above cortical amygdala (COA, $n = 11$), olfactory tubercle (OT, $n = 7$) or in piriform cortex (Pir, $n = 8$) as denoted below the site of injection. Control animals received no viral injection, and fibres implanted into cortical amygdala ($n = 4$). **d**, The percentage immobility for mice exposed to 2-phenylethanol in the absence and presence of photoactivation of bulbar axons in cortical amygdala ($n = 6$). **c**, **d**, $^{*}P < 0.05$, $^{***}P < 0.001$, paired t-test comparing with and without laser; error bars, s.e.m.

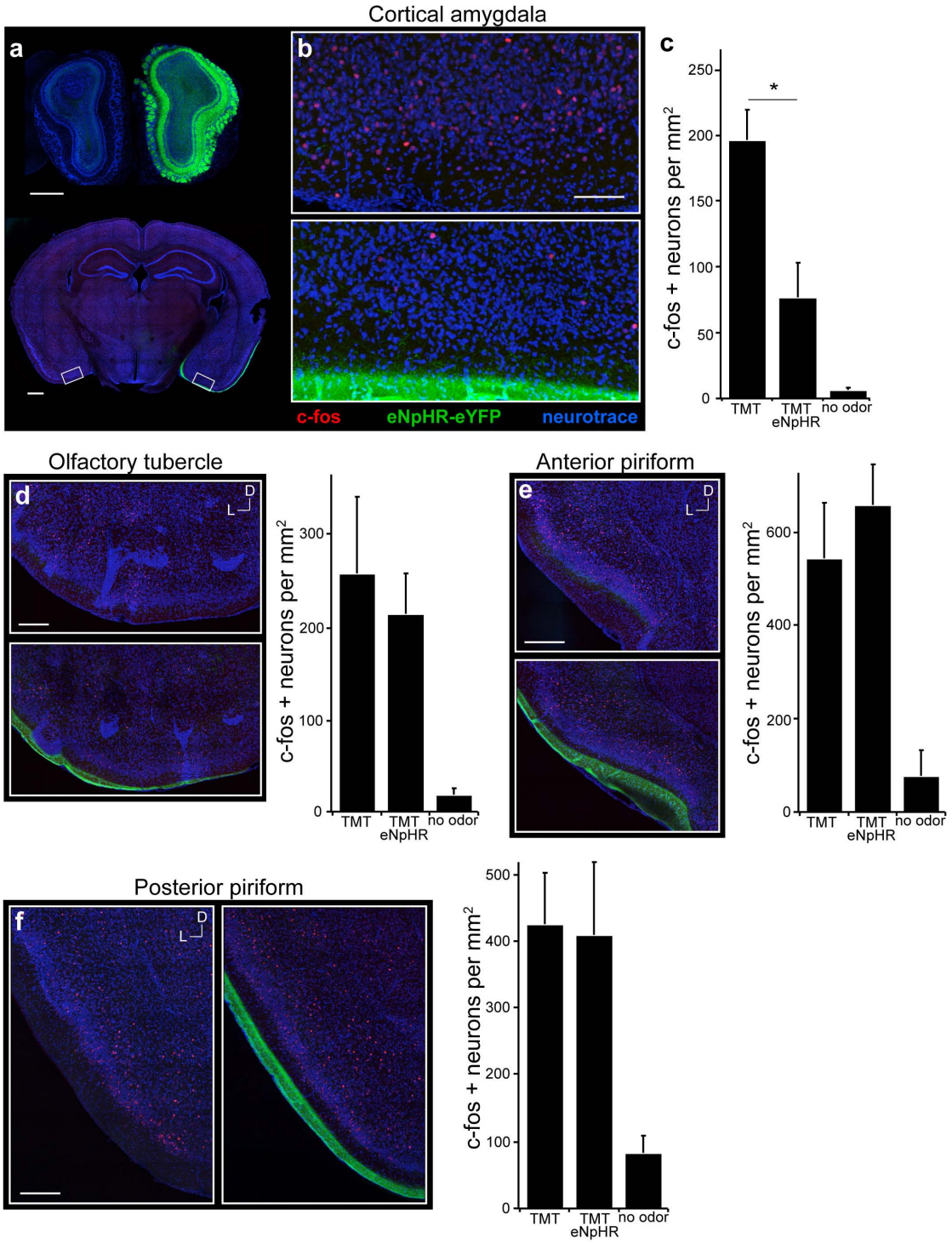

Extended Data Figure 4 | Optical suppression of bulbar input to cortical amygdala selectively reduces odour-evoked activity in this region. Mice were unilaterally injected with AAV5-eNpHR3.0–eYFP into the olfactory bulb and exposed to TMT while photoactivating the mitral-tufted cell axon terminals in cortical amygdala. **a**, Coronal section of the olfactory bulbs (top) and of the brain region with cortical amygdala (bottom) reveal halorhodopsin expression in the bulb and the lateral olfactory tract. **b**, Magnified and cropped image showing the cortical amygdala of both sides of the posterolateral cortical amygdala. The region in the bottom image received photoactivation of halorhodopsin in bulbar axon terminals during odour exposure, whereas the contralateral side (top) did not. Scale bars, 200 μm (**a**) and 100 μm (**b**). **c**, The number of neurons expressing c-fos was counted for each side of the brain ($n = 4$) as well as in control animals that did not receive any stimuli ($n = 2$) across multiple regions of cortical amygdala. Numbers are normalized by area (square millimetres) of 100 μm thick sections for comparison between brain areas. *$P < 0.05$, paired t-test comparing with and without laser; error bars, s.e.m. **d**–**f**, Coronal sections showing the olfactory tubercle (**d**), anterior piriform (**e**) and posterior piriform (**f**); the region in the bottom images received photoactivation of bulbar axon terminals in the cortical amygdala. Scale bars, 200 μm. Bar graphs show the number of neurons expressing c-fos counted for each side of the brain ($n = 4$) as well as in control animals that did not receive any stimuli ($n = 2$). Error bars, s.e.m. **a**–**f**, Images are taken from sections at the following anterior–posterior distances from bregma: −1.7 (**b**), 1.2 (**d**, **e**), −1.6 (**f**).

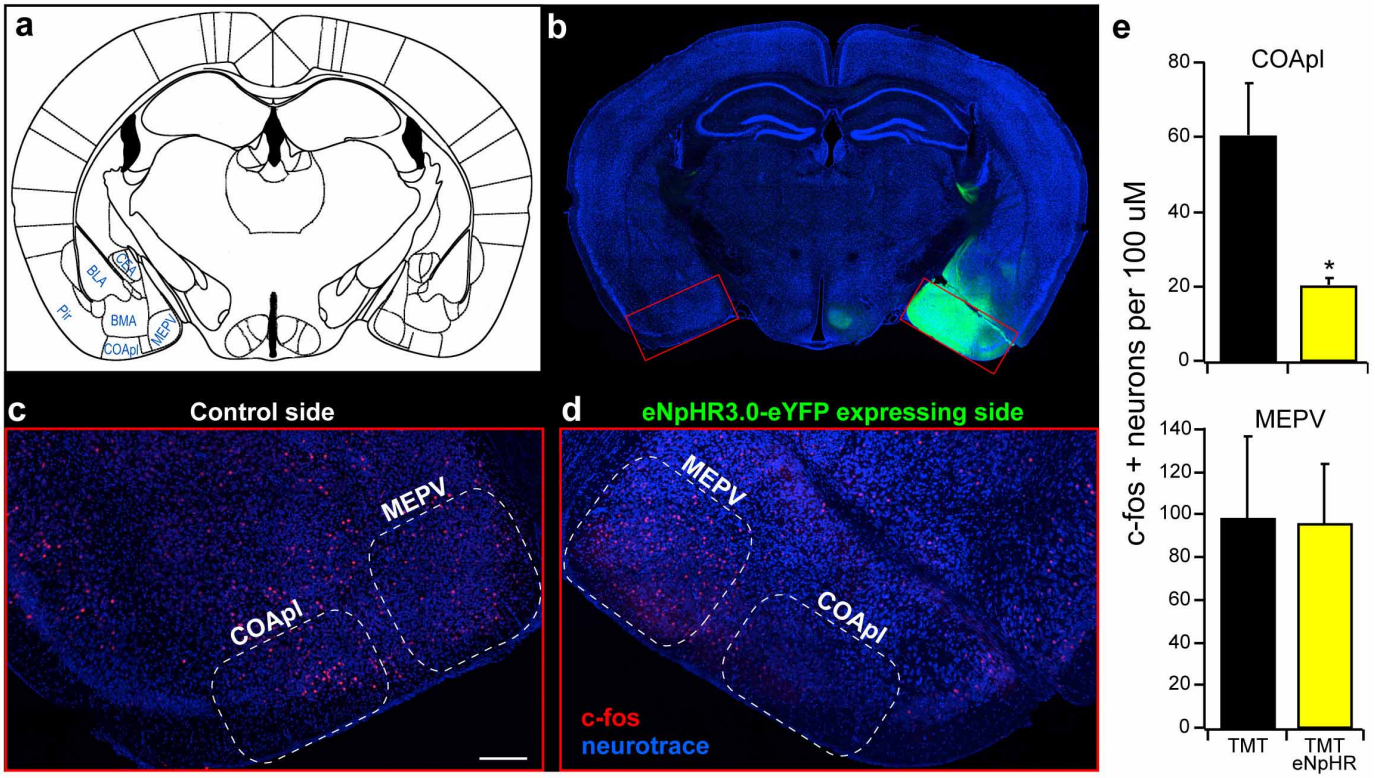

Extended Data Figure 5 | Halorhodopsin expression of neurons within cortical amygdala. Injection of AAV into cortical amygdala leads to broad expression of halorhodopsin within cortical amygdala and neighbouring areas; however, optical silencing is restricted to the cortical amygdala. **a**, Schematic of a coronal section showing cortical amygdala (COApl) in relation to other ventral brain regions. **b**–**d**, Mice were unilaterally injected with AAV5-eNpHR3.0–eYFP into the cortical amygdala and exposed to TMT while photoactivating halorhodopsin in cortical amygdala neurons. **b**, Coronal section reveals broad expression of halorhodopsin in the cortical amygdala region. This expression is broad, covering at least 90% of posterolateral cortical amygdala throughout the anterior–posterior axis. **c**, **d**, Magnified and cropped image showing c-fos expression in the cortical amygdala. The right side (**d**) received photoactivation during odour exposure, whereas the contralateral side (**c**) did not. Scale bar, 200 μm. **e**, The number of neurons expressing c-fos was counted for each side of the brain ($n = 3$) across multiple regions of the cortical amygdala (top) as well as the medial amygdala (MEPV, bottom). The mean cell number for each animal is shown in the bar graph. $^*P < 0.05$, paired *t*-test comparing with and without laser stimulation; error bars, s.e.m.

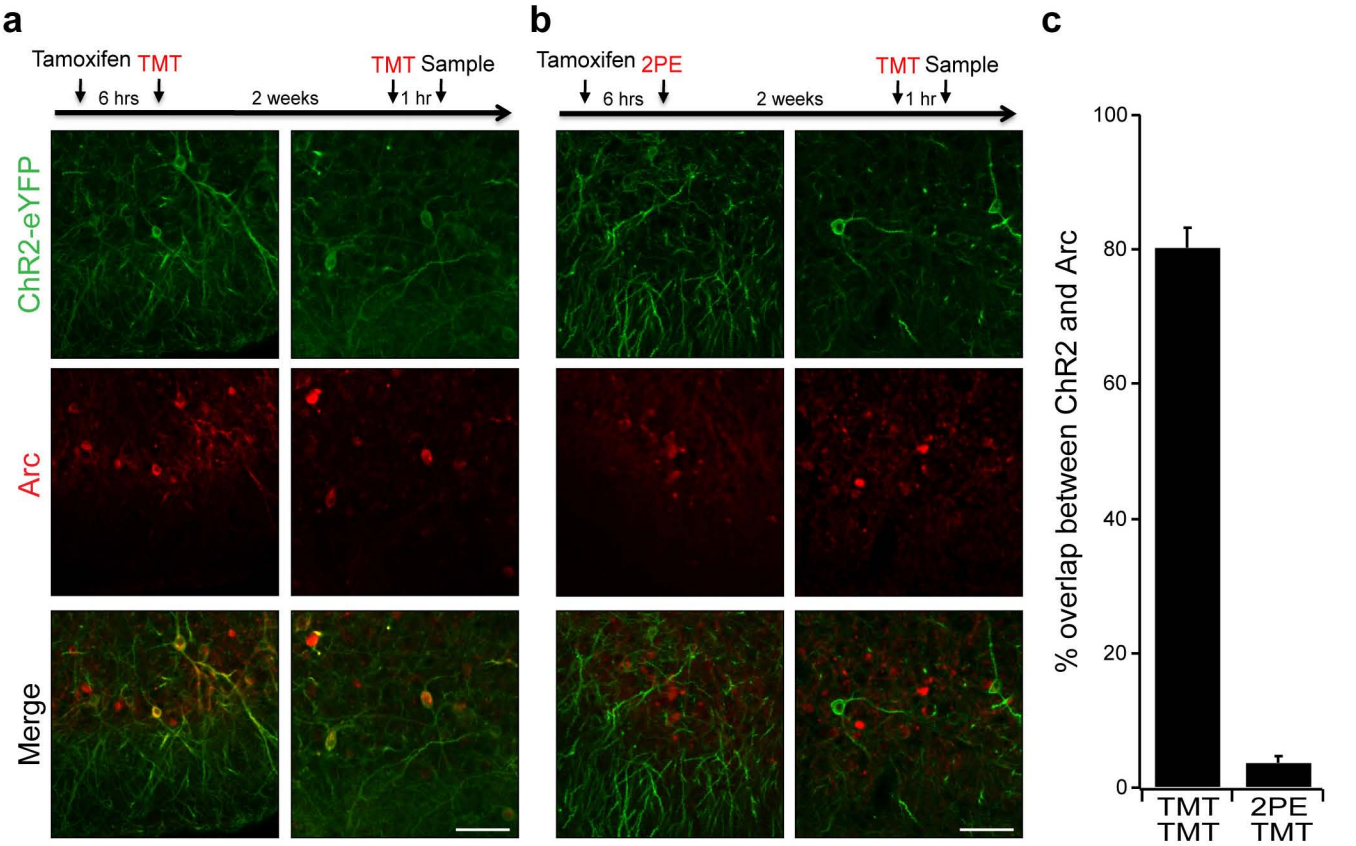

Extended Data Figure 6 | The arc promoter can be used to drive channelrhodopsin expression faithfully in odour-specific neurons. Arc-Cre-ER^{T2} mice were administered tamoxifen and exposed to odour to induce ChR2–eYFP expression, and subsequently exposed to either the same odour or a different odour and then sampled for endogenous arc expression. **a**, **b**, The timeline for odour exposure is indicated at the top, and images from two different regions of cortical amygdala are shown from representative animals for each experiment. **a**, TMT exposure induced ChR2–eYFP expression in the cortical amygdala and re-exposure to the same odour-induced arc expression detected by immunocytochemistry. **b**, 2-Phenylethanol induced expression of ChR2–eYFP followed by re-exposure to TMT. Scale bar, 100 μm. **c**, The number of channelrhodopsin-expressing neurons that also expressed the endogenous arc protein. Neurons were counted across randomly chosen sections throughout the cortical amygdala ($n = 4$).

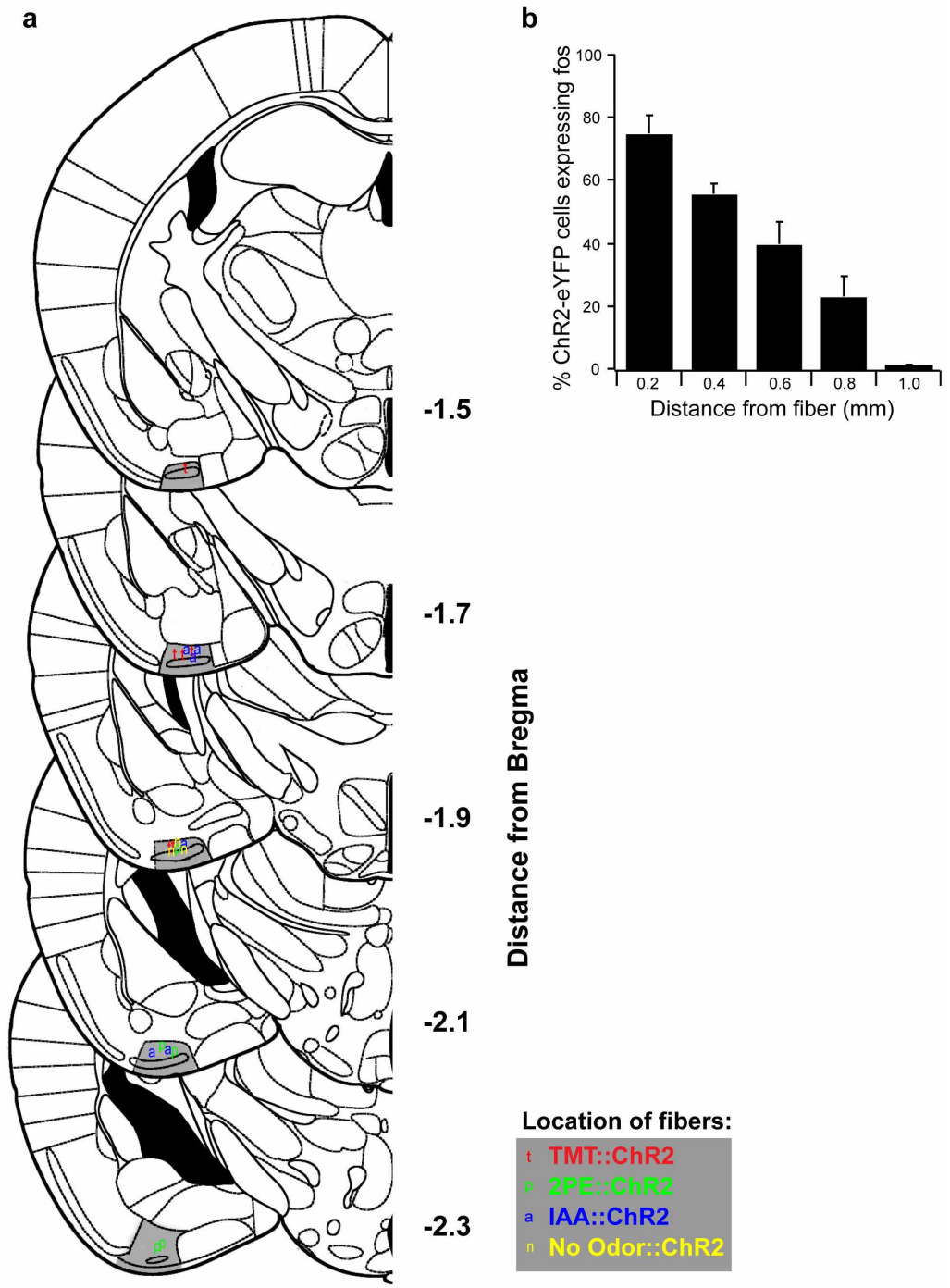

Extended Data Figure 7 | Location of optical fibres implanted in cortical amygdala for photoactivation of odour-responsive neurons. **a**, Schematics show unilateral coronal sections throughout most of the region containing cortical amygdala. The posterolateral cortical amygdala is highlighted in grey and the location of unilaterally implanted fibres is indicated. Fibres were not preferentially targeted to one side of the brain, but the fibre positions are collapsed onto unilateral schematics. **b**, The extent of light-induced activation of channelrhodopsin-expressing neurons as a function of distance from the fibre tip using c-fos expression. ArcCreER^{T2} mice were injected with AAV5-ef1α-DIO-ChR2–eYFP into cortical amygdala, administered tamoxifen and exposed to TMT to induce channelrhodopsin expression. Three weeks later, the cortical amygdala was photoactivated for 10 min with cycles of 30 s of pulsed light (10 Hz, 50% duty cycle) and 30 s off. Mice were sampled for c-fos immunoreactivity as a function of distance from the fibre tip in 200 μm bins ($n = 3$). $P < 0.001$, one-way ANOVA; error bars, s.e.m.

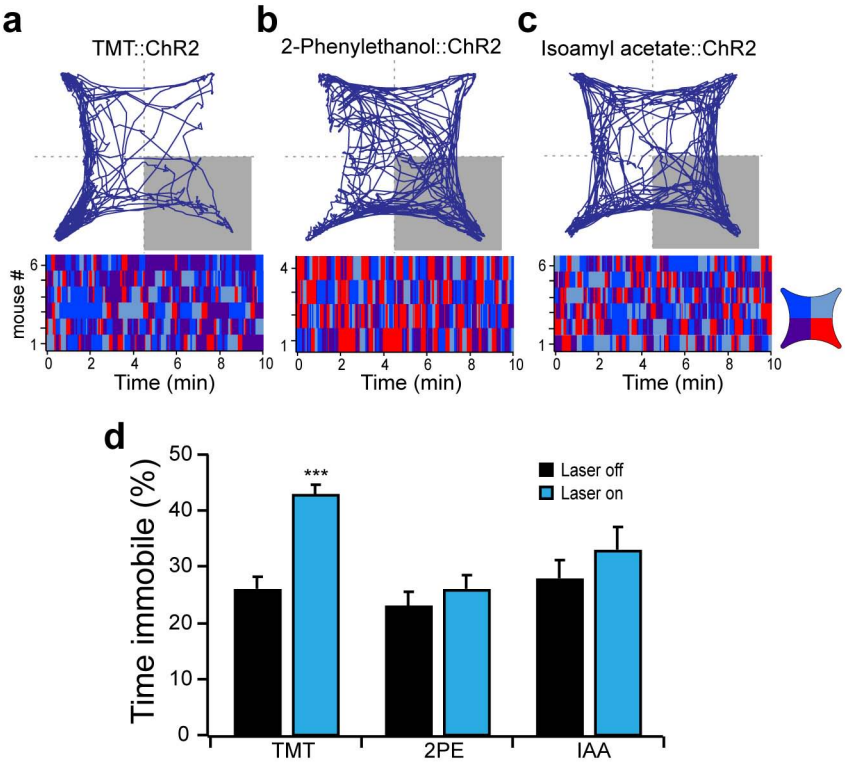

Extended Data Figure 8 | Locomotor activity of mice during activation of odour-responsive neurons within cortical amygdala. Mice with odour-driven channelrhodopsin expression were tested in the open field assay where they received pulsed photoactivation upon entrance into the lower right quadrant. **a**–**c**, The trajectory graphs (top) show the position of representative animals with ChR2–eYFP in neurons activated by TMT (**a**), 2-phenylethanol (**b**) or isoamyl acetate (**c**). The raster plots (bottom) show quadrant occupancy over time. **d**, The percentage time immobile in the absence and presence of photoactivation. Immobility is defined as velocity less than 1 cm s^{-1} for at least 1 s. **a**–**c**, TMT ($n = 6$), 2-phenylethanol ($n = 4$) and isoamyl acetate ($n = 6$); $^{***}P < 0.001$, paired t-test comparing with and without laser; error bars, s.e.m.

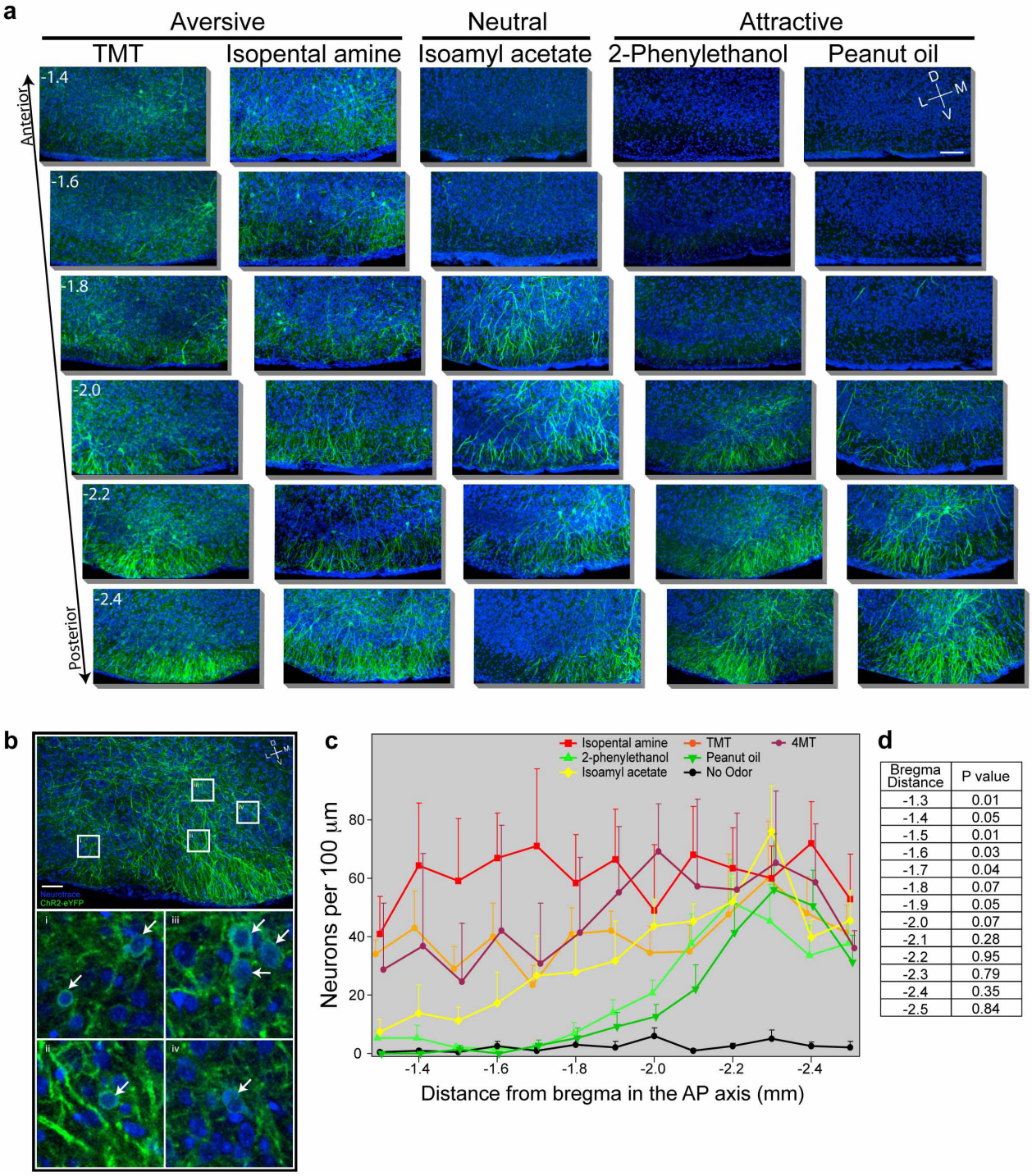

Bregma Distance	P value
-1.3	0.01
-1.4	0.05
-1.5	0.01
-1.6	0.03
-1.7	0.04
-1.8	0.07
-1.9	0.05
-2.0	0.07
-2.1	0.28
-2.2	0.95
-2.3	0.79
-2.4	0.35
-2.5	0.84

Extended Data Figure 9 | The spatial distribution of neurons responsive to different odours within cortical amgydala. **a**, ArcCreER^{T2} mice were administered tamoxifen and exposed to one of five different odours and then consecutive, serial, coronal sections were collected throughout the cortical amygdala region. Images reveal odour-driven ChR2–eYFP expression in serial sections across the cortical amygdala of representative mice for each odour. Images of the ventral brain region are magnified and cropped to show only the posterolateral cortical amygdala, and sections are displayed at 200 µm intervals across 1.2 mm of the anterior–posterior axis. Scale bar, 100 µm. **b**, Representative images showing the expression of odour-induced ChR2–eYFP with magnified images that reveal identifiable cell bodies for counting. The top image shows a *z*-projection of 40 µm through cortical amygdala (left), and the bottom images (i–iv) show magnified single *z*-plane images of small areas revealing neuronal cell bodies, indicated by the white arrows. Scale bar, 60 µm. **c**, The average number of neurons counted per 100 µm coronal section throughout the posterolateral cortical amygdala for different odours. Error bars, s.e.m. **d**, A one-way ANOVA was performed for each point along the anterior–posterior axis, comparing the means between different odours (excluding the no-odour condition). The no-odour condition was compared with each odour at −2.3 from bregma using an unpaired *t*-test; $P < 0.001$ for each odour.